Chemical Science

EDGE ARTICLE

View Article Online
View Journal | View Issue

Cite this: *Chem. Sci.*, 2019, **10**, 10531

All publication charges for this article have been paid for by the Royal Society of Chemistry

Received 24th June 2019
Accepted 24th September 2019

DOI: 10.1039/c9sc03119g

rsc.li/chemical-science

Modulating the surface defects of titanium oxides and consequent reactivity of Pt catalysts†

Yanan Wang,‡[a] Sihang Liu,‡[a] Chunlei Pei,[a] Qiang Fu,[b] Zhi-Jian Zhao,[a] Rentao Mu*[a] and Jinlong Gong*[a]

In heterogeneous catalysis, it is widely believed that the surface states of catalyst supports can strongly influence the catalytic performance, because active components are generally anchored on supports. This paper describes a detailed understanding of the influence of surface defects of TiO_2 supports on the catalytic properties of Pt catalysts. Pt was deposited on reduced (r-), hydroxylated (h-), and oxidized (o-) TiO_2 surfaces, respectively, and the different surface states of TiO_2 not only lead to differences in metal dispersion, but also distinct electronic interactions between the metal and the support. The highest reactivity for catalytic CO oxidation can be achieved over the Pt catalyst supported on reduced TiO_2 with surface oxygen vacancies. The turnover frequency (TOF) of this catalyst is determined to be ~11 times higher than that of Pt supported on oxidized TiO_2. More importantly, the reactivity is seen to increase in the sequence of Pt/o-TiO_2 < Pt/h-TiO_2 < Pt/r-TiO_2, which is well consistent with the trend of the calculated Bader charge of Pt.

Introduction

It has long been recognized that supports play an important role in heterogeneous catalysis, because supports can promote the catalytic performance and reduce the usage of noble metal catalysts.[1–5] Understanding the interfacial interaction between metals and supports, studied here, is of critical importance as metal–support interactions help the dispersion of active components and sintering resistance. Additionally, a support has also been proposed as a promoter to cause changes in the electronic structure of active components and thereby alter their catalytic properties. As such, a detailed understanding of metal interactions with supports is of high importance. Previously, extensive studies showed that metal nanoparticles and single atom catalysts exhibit variable catalytic reactivity when they are deposited on different supports, such as SiO_2, Al_2O_3, CeO_2, TiO_2, FeO_x and many others.[6–12] Surprisingly, the influence of different surface states of oxide supports on the structure and catalytic performance of metal catalysts has only been studied using model surface science systems while little is known about this factor in real supported catalysts.[13–16]

Recently, several related studies on this issue have been published. Jia and Si *et al.* discovered that the surface states of iron oxide supports, hydroxylated or dehydrated, play an important role in the performance of Au/FeO_x in CO oxidation.[17] Similarly, Wang *et al.* compared the performance of Au single atoms on perfect and defective TiO_2 nanosheet supports, in which the defective one shows a better performance in CO oxidation for a lower energy barrier and weaker competitive adsorption.[18] Furthermore, the study of Christopher *et al.* provides a detailed understanding of the structure–performance relationship of atomically dispersed catalysts.[19,20] They show that not only the intrinsic properties of metal atoms, but also the local coordination environment plays a pivotal role in the performance of catalysts.

Surface defects are ubiquitous in many materials and can affect their physical and chemical properties significantly. For example, Xie *et al.* showed that the Zn vacancies of $ZnIn_2S_4$ mediate the electron–hole separation efficiency and boost the reactivity of CO_2 reduction.[21] Surface science studies have shown that the surface defects of supports will affect the binding strength of metal atoms on them. For example, Thornton *et al.* recently unraveled the binding sites of Au atoms on a reduced TiO_2 (110) substrate, and found that bridging oxygen vacancies are the preferential anchoring sites for Au atoms.[22] Nevertheless, Buratto *et al.* discovered that the Au atoms on oxygen vacancies can be easily replaced by water molecules.[23] Besenbacher *et al.* demonstrated that oxygen adatoms bind metal atoms stronger than oxygen vacancies.[13–15]

As one of the most frequently used supports in heterogeneous catalysis, reducible oxides show a diversity of point

[a]*Key Laboratory for Green Chemical Technology of Ministry of Education, School of Chemical Engineering and Technology, Tianjin University; Collaborative Innovation Center of Chemical Science and Engineering (Tianjin), Tianjin 300072, China. E-mail: jlgong@tju.edu.cn; murt@tju.edu.cn*

[b]*State Key Laboratory of Catalysis, iChEM, Dalian Institute of Chemical Physics, Chinese Academy of Sciences, Dalian 116023, China*

† Electronic supplementary information (ESI) available: Experimental and theoretical details, supporting figures and tables. See DOI: 10.1039/c9sc03119g

‡ These authors contributed equally to this work.

defects at surfaces, such as oxygen vacancies, hydroxyls, oxygen adatoms, *etc.* It has been demonstrated that these defects are fragile, environmentally sensitive and facile to transform from one to another. For example, the oxygen vacancies at the surface of many oxides can interact with water molecules and easily break them into two hydroxyl groups.[24–28] Upon annealing treatment in a vacuum or a reductive atmosphere, hydroxyls will recombine into water again, forming a reduced surface with oxygen vacancies.[29] Consequently, direct studies of the influence of a specific kind of surface defect on the catalytic reactivity remain a great challenge, in particular for catalysts supported on oxide nanoparticles.

This paper focuses on the influence of different surface defects of TiO_2 supports on the catalytic properties of Pt catalysts, because Pt/TiO_2 has been extensively used in heterogeneous catalysis, photocatalytic water splitting, and electrochemistry.[30–34] By finely tuning the surface states of TiO_2, we prepare Pt catalysts deposited on reduced (r-), hydroxylated (h-) and oxidized (o-) surfaces, respectively. It is shown that the surface states of TiO_2 not only influence the degree of metal dispersion, but also change the electronic metal–support interactions which affect the catalytic properties of Pt directly.

Results and discussion

Modulating the surface states of TiO_2 supports

TiO_2 supports with different surface states were prepared in a specific atmosphere. The detailed preparation process is given in Fig. S1.† First, commercial rutile TiO_2 was calcined in Ar and O_2 to remove contaminants, such as carbonate and moisture. To prepare a reduced surface, TiO_2 was treated in an Ar atmosphere at 700 °C for 1 h.[35] Upon the exposure of r-TiO_2 to water vapor at 130 °C for 1 h, a hydroxylated surface can be obtained. At this temperature, the molecular water should be desorbed.[36] On the other hand, oxidized TiO_2 was prepared by exposing r-TiO_2 to O_2 at room temperature. X-ray diffraction (XRD) results (Fig. 1A and Table S1†) show the same peak position and peak shape over the different TiO_2 supports, indicating that their bulk structures are the same. Additionally, the E_g peak and full width at half maximum (FWHM) in visible Raman spectra (Fig. 1B and Table S2†) do not change after the hydroxylation and oxidation of reduced TiO_2, which also indicates that the bulk states of the different TiO_2 samples should be the same.[37,38]

To understand the surface states of TiO_2, X-ray photoelectron spectroscopy (XPS) was carried out (Fig. 1C). The binding energy (BE) of XPS Ti $2p_{3/2}$ on hydroxylated and oxidized surfaces is 459.3 eV, which can be assigned to Ti^{4+}.[39,40] Over reduced TiO_2, a small shoulder peak at a lower BE of 457.5 eV is observed, which indicates the presence of the Ti^{3+} state on the reduced surface.[39,40] When r-TiO_2 was exposed to water vapor, a small shoulder peak at a higher BE of the O 1s peak appears (Fig. S2A†), suggesting the formation of surface hydroxyl groups *via* H_2O dissociation at oxygen vacancies.[41] Upon the exposure of r-TiO_2 to O_2, the oxygen vacancies should be filled and oxygen adatoms will be generated on the top of regular Ti_{5c} sites (Fig. S2B†). The dissociation mechanism of O_2 on TiO_2 was clarified in previous investigations.[42–44] The disappearance of the XPS Ti^{3+} peak on h-TiO_2 and o-TiO_2 further indicates that the dissociative adsorption of water and O_2 can occur at oxygen vacancies.

Preparation of Pt/TiO_2 catalysts

To prepare Pt catalysts on different supports, the pre-treated TiO_2 was transferred into a glove box filled with Ar, and thus the surface states of pre-treated TiO_2 will remain unchanged. In order to exclude the influence of O_2, water and other contaminants in air during the preparation process, Pt/TiO_2 catalysts were also synthesized in a glove box under the protection of an Ar atmosphere.

The influence of surface states of TiO_2 on the dispersion of Pt catalysts was determined by chemisorption, high-angle annular dark-field scanning transmission electron microscopy (HAADF-STEM) and XPS measurements. The CO chemisorption and H_2–O_2 titration results suggest that the dispersion of Pt catalysts is highest on r-TiO_2, followed by Pt/h-TiO_2 and Pt/o-TiO_2 (Tables 1 and S3†). From HAADF-STEM studies (Fig. 2), it was found that the Pt nanoparticles on r-TiO_2 present uniform size distribution with an average diameter of 1.19 nm. In contrast, larger Pt nanoparticles are observed on h-TiO_2 (1.56 nm) and o-TiO_2 (1.61 nm). For the size distribution of catalysts after reaction (1.46 ± 0.36 nm, 1.46 ± 0.39 nm and 1.61 ± 0.43 nm for Pt/r-TiO_2, Pt/h-TiO_2 and Pt/o-TiO_2, respectively), only a small variation of particle size can be observed. From XPS investigations (Table

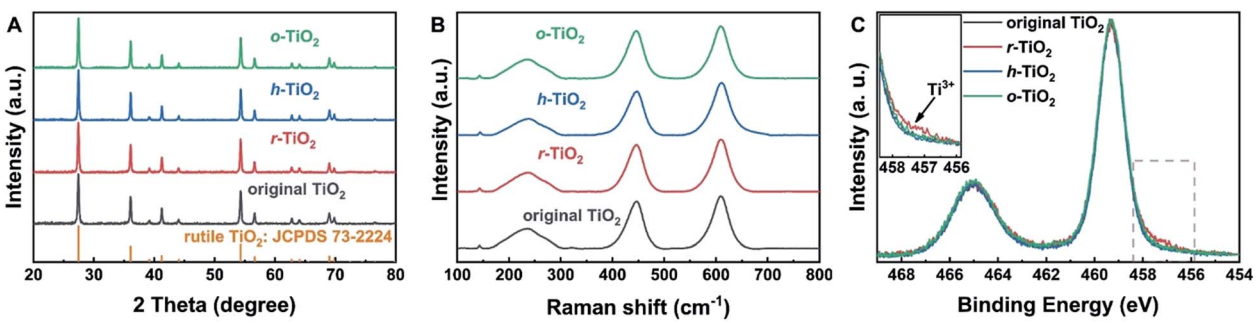

Fig. 1 Bulk and surface properties of TiO_2 supports. (A) XRD patterns of different TiO_2 supports; (B) Raman spectra of different TiO_2 supports; (C) XPS Ti 2p peaks of different TiO_2 supports. The inset in (C) shows the Ti^{3+} species on reduced TiO_2.

Table 1 Catalytic properties of different catalysts

Sample	Dispersion[a]	Specific rate × 100[b] (mol CO/(g Pt·h))	TOF_a × 100[c] (s^{-1})	TOF_b × 100[d] (s^{-1})
Pt/r-TiO_2	86%	226	14.2	200.2
Pt/h-TiO_2	53%	81	8.2	187.0
Pt/o-TiO_2	36%	8	1.3	42.6

[a] The dispersion is tested by CO chemisorption. [b] The specific rate is derived from the CO conversion at 80 °C. [c] The TOF_a is calculated based on the dispersion of metal nanoparticles. [d] The TOF_b is calculated based on the length of the perimeter between Pt nanoparticles and TiO_2.

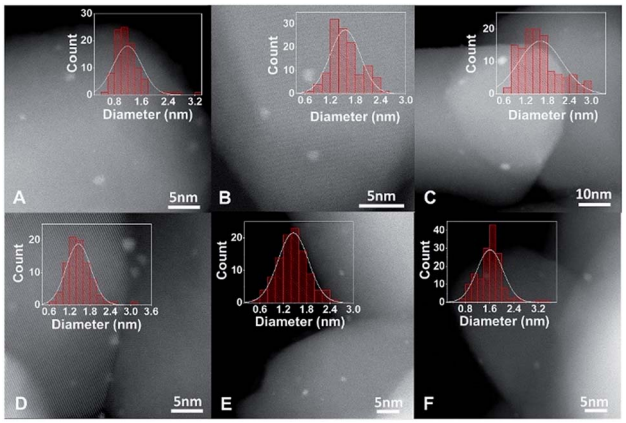

Fig. 2 HAADF-STEM and size distribution of Pt/TiO_2 catalysts. (A–C) and (D–F) are HADDF-STEM and size distribution of Pt/r-TiO_2, Pt/h-TiO_2 and Pt/o-TiO_2 before and after reaction, respectively.

S4†), it was found that the Pt/r-TiO_2 catalyst shows a stronger normalized peak area of Pt 4f/Ti 2p than Pt/h-TiO_2 and Pt/o-TiO_2, indicating that the Pt nanoparticles are more highly dispersed on r-TiO_2. The results from H_2–O_2 titration, CO chemisorption, HAADF-STEM and XPS are well consistent with each other, which illustrates that the dispersion of Pt catalysts increases in the sequence of Pt/o-TiO_2 < Pt/h-TiO_2 < Pt/r-TiO_2.

Catalytic performance

The reactivity to CO oxidation was comparatively studied over the different catalysts (Fig. 3A). Not surprisingly, the best reactivity is observed on Pt/r-TiO_2. With this catalyst, 50% CO conversion takes place at 87.6 °C. In contrast, the Pt/h-TiO_2 and Pt/o-TiO_2 catalysts exhibit worse performance, in which 50% CO conversion occurs at 102.3 and 126.3 °C, respectively. It is noteworthy that a similar trend of CO oxidation reactivity can be observed over the catalysts with different concentrations of surface defects, which are prepared through different treatment times (Fig. S3 and S4†).

The kinetic measurement of CO oxidation was further conducted. It can be found that the specific rate of Pt/r-TiO_2 to CO oxidation is ~2.8 and ~28 times higher than that of Pt/h-TiO_2 and Pt/o-TiO_2, respectively (Table 1). In addition, the turnover frequency (TOF) values based on the surface area (TOF_a) and the perimeter length of Pt nanoparticles (TOF_b) are shown in Tables 1 and S3.† The Pt/r-TiO_2 catalyst shows a TOF_a of 0.142 s^{-1} and a TOF_b of 2.002 s^{-1}, while the Pt/h-TiO_2 and Pt/o-TiO_2 catalysts exhibit much lower values. For the CO oxidation reaction occurring over noble metal catalysts, many previous studies suggested that the reaction obeys the Mars–van Krevelen (M–vK) mechanism on reducible catalysts or the Langmuir–Hinshelwood (L–H) mechanism on non-reducible catalysts.[30,45–47] The reaction order test shows that the orders of CO and O_2 on different catalysts are almost the same, negative for CO and near to zero for O_2 (Fig. S5†), which is consistent with the M–vK mechanism. Furthermore, the comparable apparent activation energy (E_a) derived from the Arrhenius plot demonstrates that the CO oxidation on the different catalysts should follow the same reaction mechanism (Fig. 3B).

Electronic metal–support interactions

It has been generally agreed that supported Pt catalysts show low structure sensitivity for CO oxidation. For example, Iglesia and Lu *et al.* suggested that the catalytic properties of Pt/Al_2O_3 and Pt/TiO_2 catalysts for CO oxidation are independent of Pt cluster size.[30,47] Although theoretical calculations and surface

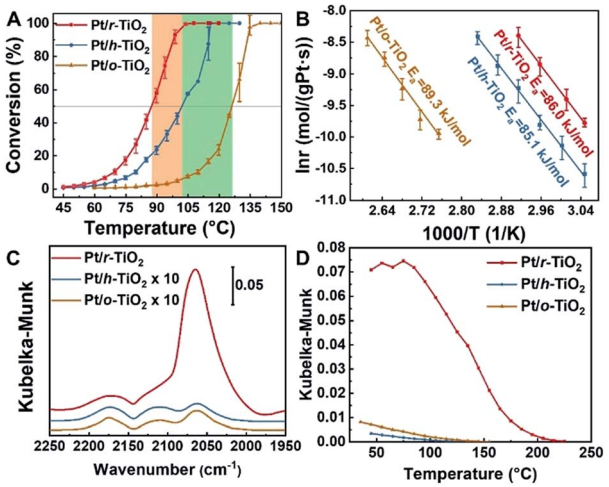

Fig. 3 Reactivity, kinetic properties and DRIFTS of CO adsorption on Pt/TiO_2 catalysts. (A) Light-off curves of CO conversion on different catalysts. The CO oxidation was conducted with a gas composition of 1% CO, 20% O_2 and He balanced, keeping GHSV at 18 000 ml $g_{cat.}^{-1}$ h^{-1}. Each point is tested at a fixed temperature three times and then ramped to higher temperature. (B) Arrhenius plot of CO oxidation on different catalysts. (C) DRIFTS in CO oxidation (1% CO, 20% O_2 and He balanced) at 80 °C. The spectra were acquired after 5 minutes of reaction. (D) Plot of CO adsorption amount as a function of temperature in an Ar atmosphere. CO was pre-adsorbed at room temperature.

science experiments suggested that the reaction should be highly structure sensitive,[48–50] Christopher *et al.* showed that CO-induced structure reconstruction of Pt nanoparticles mitigates the inherent structure sensitivity.[51] Therefore, the observed reactivity difference of Pt/TiO_2 catalysts can be attributed to the different electronic metal–support interactions.

From XPS studies of nano-sized materials, it was found that the final state effect will make BE shift to a higher position for smaller metal nanoparticles.[52–54] Although the size of Pt nanoparticles on r-TiO_2 is smaller than that on h-TiO_2 and o-TiO_2, the BE of XPS Pt $4f_{7/2}$ peaks from Pt/r-TiO_2 is even ~0.2 eV lower than that from Pt/h-TiO_2 (Fig. S6, S7 and Table S4†). This indicates that Pt may accept more electrons from r-TiO_2 or transfer fewer electrons to r-TiO_2 compared to Pt/h-TiO_2 and Pt/o-TiO_2 catalysts.

Diffuse reflection infrared Fourier transform spectroscopy (DRIFTS) of CO adsorption was also conducted to demonstrate the electronic metal–support interactions. It can be found that the better catalyst for CO oxidation shows a larger amount of CO adsorption in Kubelka–Munk units, which are assumed to be linearly related to the adsorbate coverage (Fig. 3C).[4,55] Besides the larger CO adsorption amount, the Pt/r-TiO_2 catalyst also presents ~80 °C higher temperature for complete CO desorption compared to Pt/h-TiO_2 and Pt/o-TiO_2, which indicates that CO binds stronger with Pt/r-TiO_2 (Fig. 3D). The higher CO coverage induced by electronic interactions should be detrimental to the reactivity of Pt/r-TiO_2 in kinetic aspects due to the negative reaction order. However, Pt/r-TiO_2 shows better reactivity than Pt/h-TiO_2 and Pt/o-TiO_2. Therefore, it can be drawn that electronic interactions play a dominant role thermodynamically in reactivity modulation which is demonstrated by the DFT calculations.

Theoretical calculations

Density functional theory (DFT) calculations provide further insights into the electronic interactions between metals and supports, and their influence on catalytic reactivity. Bader charge analysis shows that the average charges of Pt on r-TiO_2, h-TiO_2 and o-TiO_2 are determined to be +0.04, +0.08 and +0.10, respectively (Fig. S8†), which agrees with XPS measurements.

The CO adsorbed at the interface of Pt/r-TiO_2 is found to have a binding energy of 2.08 eV, which is 0.29 and 0.21 eV higher than those for the CO adsorbed at the interface of Pt/h-TiO_2 and Pt/o-TiO_2, respectively. This result is well consistent with the DRIFTS results. Furthermore, the reaction barriers of adsorbed CO with the lattice oxygen of TiO_2 (CO + O) were also calculated. Fig. 4 shows the energy barriers and TS geometries for CO oxidation on the different catalysts. It can be found that the energy barriers for the CO reaction are 0.89 eV, 0.96 eV and 1.04 eV on Pt/r-TiO_2, Pt/h-TiO_2 and Pt/o-TiO_2, respectively. The barrier is consistent with E_a derived from the kinetic test (~0.95 eV). However, compared with the reaction path on Pt/h-TiO_2 and Pt/o-TiO_2, the route on Pt/r-TiO_2 is energetically more favorable which is downhill for further CO_2 desorption and the free energy barrier of the CO oxidation process is also slightly

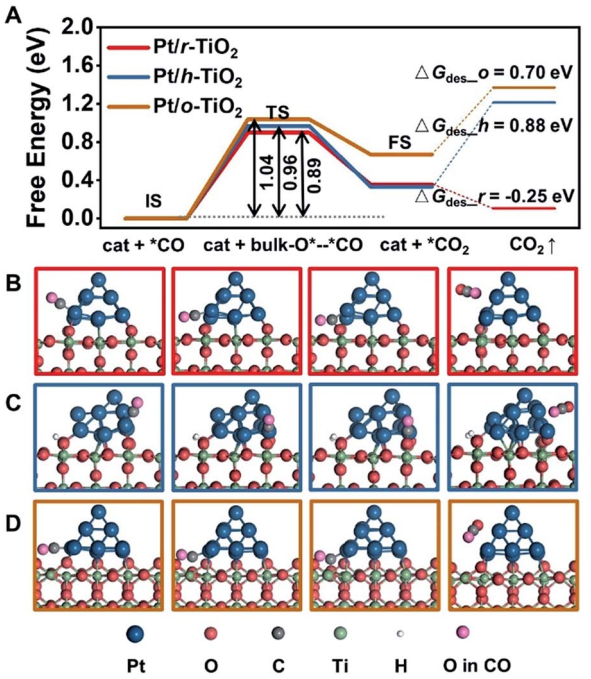

Fig. 4 Calculated CO oxidation over Pt/TiO_2 catalysts. (A) Free energy barriers for CO oxidation. (B–D) Models from left to right represent the initial state (IS), transition state (TS), final state (FS) and CO_2 desorption of CO oxidation on Pt/r-TiO_2, Pt/h-TiO_2 and Pt/o-TiO_2, respectively.

favored. This indicates that Pt/r-TiO_2 should exhibit better reactivity for CO oxidation than Pt/h-TiO_2 and Pt/o-TiO_2. Subsequently, the reaction barriers for CO oxidation on different Pt/TiO_2 surfaces with oxygen vacancies (CO + O_2 + O_vac) were calculated (Fig. S9†). It can be seen that the reaction barriers for CO + O_2 + O_vac are much lower than those for CO + O over different catalysts.

Conclusions

Although it has been known that the surface states of supports should play an important role in the catalytic properties of catalysts, an understanding of the correlation between the surface states of supports and catalytic performance is still lacking, especially for real supported catalytic systems. Surface science investigations have shown that metal nanoparticles can be trapped at O adatoms and O vacancies on the TiO_2 (110) surface under ultra-high vacuum conditions.[13–15,22] However, in practice, the influence of air atmosphere and the structural complexity has made direct studies of real supported catalysts very difficult. In the present study, the preparation of different catalysts was carried out under the protection of an Ar atmosphere, and thus the influence of active molecules (O_2, H_2O, *etc.*) in air can be excluded, but this was often ignored before.

In summary, we demonstrate how sensitively the catalytic performance of Pt catalysts depends on the surface states of TiO_2 supports. Before depositing Pt catalysts, different TiO_2 supports, including reduced, hydroxylated and oxidized types, were obtained *via* pre-treatments in different atmospheres. The

highest reactivity for CO oxidation was achieved using Pt catalysts supported on r-TiO_2, whereas worse performance was seen for the catalysts supported on h-TiO_2 and o-TiO_2. The established surface state–electronic structure–reactivity relationship clearly illustrates the important role of surface defects in catalytic performance and can be readily extended to many other metal/oxide catalytic systems.

Conflicts of interest

There are no conflicts to declare.

Acknowledgements

This work was financially supported by the National Key Research and Development Program of China (No. 2016YFB0600901), the National Science Foundation of China (No. 21525626, 91645106, and 21603159) and the Program of Introducing Talents of Discipline to Universities (No. B06006). We thank Jie Xu and Prof. Jun Luo from Tianjin University of Technology for HADDF-STEM characterization and Chao Wang from Dalian Institute of Chemical Physics for XPS characterization. We also thank Hao Li from Tianjin University, and Dr Lijun Gao and Dr Jinhu Dong from Dalian Institute of Chemical Physics for fruitful discussions.

References

1 M. Ahmadi, H. Mistry and B. Roldan Cuenya, *J. Phys. Chem. Lett.*, 2016, **7**, 3519–3533.
2 F. Shi, L. R. Baker, A. Hervier, G. A. Somorjai and K. Komvopoulos, *Nano Lett.*, 2013, **13**, 4469–4474.
3 N. J. Divins, I. Angurell, C. Escudero, V. Pérez-Dieste and J. Llorca, *Science*, 2014, **346**, 620–623.
4 Y. Wang, D. Widmann and R. J. Behm, *ACS Catal.*, 2017, **7**, 2339–2345.
5 Y. Wang, D. Widmann, M. Heenemann, T. Diemant, J. Biskupek, R. Schlögl and R. J. Behm, *J. Catal.*, 2017, **354**, 46–60.
6 K. Ding, A. Gulec, A. M. Johnson, N. M. Schweitzer, G. D. Stucky, L. D. Marks and P. C. Stair, *Science*, 2015, **350**, 189–192.
7 M. Moses-DeBusk, M. Yoon, L. F. Allard, D. R. Mullins, Z. Wu, X. Yang, G. Veith, G. M. Stocks and C. K. Narula, *J. Am. Chem. Soc.*, 2013, **135**, 12634–12645.
8 L. Nie, D. Mei, H. Xiong, B. Peng, Z. Ren, X. I. P. Hernandez, A. DeLaRiva, M. Wang, M. H. Engelhard, L. Kovarik, A. K. Datye and Y. Wang, *Science*, 2017, **358**, 1419–1423.
9 D. A. J. M. Ligthart, R. A. van Santen and E. J. M. Hensen, *Angew. Chem., Int. Ed.*, 2011, **50**, 5306–5310.
10 H. Li, S. Zha, Z.-J. Zhao, H. Tian, S. Chen, Z. Gong, W. Cai, Y. Wang, Y. Cui, L. Zeng, R. Mu and J. Gong, *ACS Catal.*, 2018, **8**, 5526–5532.
11 B. Qiao, A. Wang, X. Yang, L. F. Allard, Z. Jiang, Y. Cui, J. Liu, J. Li and T. Zhang, *Nat. Chem.*, 2011, **3**, 634–641.
12 Y. Lou and J. Liu, *Ind. Eng. Chem. Res.*, 2017, **56**, 6916–6925.
13 D. Matthey, J. G. Wang, S. Wendt, J. Matthiesen, R. Schaub, E. Lægsgaard, B. Hammer and F. Besenbacher, *Science*, 2007, **315**, 1692–1696.
14 J. Ø. Hansen, E. Lira, P. Galliker, J.-G. Wang, P. T. Sprunger, Z. Li, E. Lægsgaard, S. Wendt, B. Hammer and F. Besenbacher, *J. Phys. Chem. C*, 2010, **114**, 16964–16972.
15 F. Rieboldt, L. B. Vilhelmsen, S. Koust, J. V. Lauritsen, S. Helveg, L. Lammich, F. Besenbacher, B. Hammer and S. Wendt, *J. Chem. Phys.*, 2014, **141**, 214702.
16 S. Bonanni, K. Aït-Mansour, W. Harbich and H. Brune, *J. Am. Chem. Soc.*, 2012, **134**, 3445–3450.
17 H.-Z. Cui, Y. Guo, X. Wang, C.-J. Jia and R. Si, *Catalysts*, 2016, **6**, 37.
18 J. Wan, W. Chen, C. Jia, L. Zheng, J. Dong, X. Zheng, Y. Wang, W. Yan, C. Chen, Q. Peng, D. Wang and Y. Li, *Adv. Mater.*, 2018, **30**, 1705369.
19 L. DeRita, J. Resasco, S. Dai, A. Boubnov, H. V. Thang, A. S. Hoffman, I. Ro, G. W. Graham, S. R. Bare, G. Pacchioni, X. Pan and P. Christopher, *Nat. Mater.*, 2019, **18**, 746–751.
20 E. C. H. Sykes, *Nat. Mater.*, 2019, **18**, 663–664.
21 X. Jiao, Z. Chen, X. Li, Y. Sun, S. Gao, W. Yan, C. Wang, Q. Zhang, Y. Lin, Y. Luo and Y. Xie, *J. Am. Chem. Soc.*, 2017, **139**, 7586–7594.
22 A. Mellor, D. Humphrey, C. M. Yim, C. L. Pang, H. Idriss and G. Thornton, *J. Phys. Chem. C*, 2017, **121**, 24721–24725.
23 X. Tong, L. Benz, S. Chrétien, H. Metiu, M. T. Bowers and S. K. Buratto, *J. Phys. Chem. C*, 2010, **114**, 3987–3990.
24 O. Bikondoa, C. L. Pang, R. Ithnin, C. A. Muryn, H. Onishi and G. Thornton, *Nat. Mater.*, 2006, **5**, 189–192.
25 S. Wendt, J. Matthiesen, R. Schaub, E. K. Vestergaard, E. Lægsgaard, F. Besenbacher and B. Hammer, *Phys. Rev. Lett.*, 2006, **96**, 066107.
26 R. Mu, D. C. Cantu, X. Lin, V.-A. Glezakou, Z. Wang, I. Lyubinetsky, R. Rousseau and Z. Dohnálek, *J. Phys. Chem. Lett.*, 2014, **5**, 3445–3450.
27 R. Mu, D. C. Cantu, V.-A. Glezakou, I. Lyubinetsky, R. Rousseau and Z. Dohnálek, *J. Phys. Chem. C*, 2015, **119**, 23552–23558.
28 Z.-T. Wang, Y.-G. Wang, R. Mu, Y. Yoon, A. Dahal, G. K. Schenter, V.-A. Glezakou, R. Rousseau, I. Lyubinetsky and Z. Dohnálek, *Proc. Natl. Acad. Sci. U. S. A.*, 2017, **114**, 1801–1805.
29 R. Mu, Z.-j. Zhao, Z. Dohnalek and J. Gong, *Chem. Soc. Rev.*, 2017, **46**, 1785–1806.
30 N. Li, Q.-Y. Chen, L.-F. Luo, W.-X. Huang, M.-F. Luo, G.-S. Hu and J.-Q. Lu, *Appl. Catal., B*, 2013, **142–143**, 523–532.
31 G. T. K. K. Gunasooriya, E. G. Seebauer and M. Saeys, *ACS Catal.*, 2017, **7**, 1966–1970.
32 M. Ni, M. K. H. Leung, D. Y. C. Leung and K. Sumathy, *Renewable Sustainable Energy Rev.*, 2007, **11**, 401–425.
33 J. Yu, L. Qi and M. Jaroniec, *J. Phys. Chem. C*, 2010, **114**, 13118–13125.
34 S. Xie, Y. Wang, Q. Zhang, W. Deng and Y. Wang, *ACS Catal.*, 2014, **4**, 3644–3653.
35 S. Wendt, R. Schaub, J. Matthiesen, E. K. Vestergaard, E. Wahlström, M. D. Rasmussen, P. Thostrup,

L. M. Molina, E. Lægsgaard, I. Stensgaard, B. Hammer and F. Besenbacher, *Surf. Sci.*, 2005, **598**, 226–245.
36 J. Ø. Hansen, J. Matthiesen, E. Lira, L. Lammich and S. Wendt, *Surf. Sci.*, 2017, **666**, 113–122.
37 J. C. Parker and R. W. Siegel, *Appl. Phys. Lett.*, 1990, **57**, 943–945.
38 H. Zhang, J. Cai, Y. Wang, M. Wu, M. Meng, Y. Tian, X. Li, J. Zhang, L. Zheng, Z. Jiang and J. Gong, *Appl. Catal., B*, 2018, **220**, 126–136.
39 A. N. Shultz, W. Jang, W. M. Hetherington, D. R. Baer, L.-Q. Wang and M. H. Engelhard, *Surf. Sci.*, 1995, **339**, 114–124.
40 F. Guillemot, M. C. Porté, C. Labrugère and C. Baquey, *J. Colloid Interface Sci.*, 2002, **255**, 75–78.
41 J. Balajka, M. A. Hines, W. J. I. DeBenedetti, M. Komora, J. Pavelec, M. Schmid and U. Diebold, *Science*, 2018, **361**, 786–789.
42 Y. Du, Z. Dohnálek and I. Lyubinetsky, *J. Phys. Chem. C*, 2008, **112**, 2649–2653.
43 Z.-T. Wang, Y. Du, Z. Dohnálek and I. Lyubinetsky, *J. Phys. Chem. Lett.*, 2010, **1**, 3524–3529.
44 E. Lira, J. Ø. Hansen, P. Huo, R. Bechstein, P. Galliker, E. Lægsgaard, B. Hammer, S. Wendt and F. Besenbacher, *Surf. Sci.*, 2010, **604**, 1945–1960.
45 S. T. Daniells, A. R. Overweg, M. Makkee and J. A. Moulijn, *J. Catal.*, 2005, **230**, 52–65.
46 M. Kotobuki, R. Leppelt, D. A. Hansgen, D. Widmann and R. J. Behm, *J. Catal.*, 2009, **264**, 67–76.
47 A. D. Allian, K. Takanabe, K. L. Fujdala, X. Hao, T. J. Truex, J. Cai, C. Buda, M. Neurock and E. Iglesia, *J. Am. Chem. Soc.*, 2011, **133**, 4498–4517.
48 T. Jiang, D. J. Mowbray, S. Dobrin, H. Falsig, B. Hvolbæk, T. Bligaard and J. K. Nørskov, *J. Phys. Chem. C*, 2009, **113**, 10548–10553.
49 S. Bonanni, K. Aït-Mansour, W. Harbich and H. Brune, *J. Am. Chem. Soc.*, 2014, **136**, 8702–8707.
50 O. Balmes, G. Prevot, X. Torrelles, E. Lundgren and S. Ferrer, *ACS Catal.*, 2016, **6**, 1285–1291.
51 M. J. Kale and P. Christopher, *ACS Catal.*, 2016, **6**, 5599–5609.
52 M. Turner, V. B. Golovko, O. P. H. Vaughan, P. Abdulkin, A. Berenguer-Murcia, M. S. Tikhov, B. F. G. Johnson and R. M. Lambert, *Nature*, 2008, **454**, 981.
53 D. P. Anderson, J. F. Alvino, A. Gentleman, H. A. Qahtani, L. Thomsen, M. I. J. Polson, G. F. Metha, V. B. Golovko and G. G. Andersson, *Phys. Chem. Chem. Phys.*, 2013, **15**, 3917–3929.
54 W. E. Kaden, T. Wu, W. A. Kunkel and S. L. Anderson, *Science*, 2009, **326**, 826–829.
55 T. Armaroli, T. Bécue and S. Gautier, *Oil Gas Sci. Technol.*, 2004, **59**, 215–237.